Design and Initial Testing of an Ex-Core Fast Neutron Irradiator for the UMass-Lowell Research Reactor

John R. White and Areeya Jirapongmed
Chemical and Nuclear Engineering Department

Leo Bobek and Thomas M. Regan
Radiation Laboratory

University of Massachusetts Lowell

Lowell, MA 01854

Presented at

Radiation Protection and Shielding Topical Conference
Santa Fe, New Mexico

April 14-18, 2002

DESIGN AND INITIAL TESTING OF AN EX-CORE FAST NEUTRON IRRADIATOR FOR THE UMASS-LOWELL RESEARCH REACTOR

John R. White and Areeya Jirapongmed
Chemical and Nuclear Engineering Department
University of Massachusetts Lowell
Lowell, MA 01854
John_White@uml.edu
Areeya_Jirapongmed@student.uml.edu

Leo Bobek and Thomas Regan
Radiation Laboratory
University of Massachusetts Lowell
Lowell, MA 01854
Leo_Bobek@uml.edu
Thomas_Regan@uml.edu

SUMMARY
A new ex-core fast neutron irradiation facility has recently been installed within the pool of the University of Massachusetts Lowell Research Reactor. This new experimental facility replaces the three beam ports that originally existed on one side of the core. It gives a fast flux level greater than 10^{11} n/cm^2-s, with relatively low thermal fluence and gamma dose rates. Samples with a cross-sectional area as large as 12"x12" and up to 6" thick can be irradiated within the new facility. The fast neutron flux is nearly uniform over the 12"x12" area facing the core, and the fast fluence variation through the sample thickness is minimized via a single 180^o rotation of the sample canister at the midpoint of the irradiation period. This new fast neutron irradiation facility offers a significantly larger sample volume than previously available within the Radiation Laboratory at UMass-Lowell.

I. INTRODUCTION

The 1 MWth University of Massachusetts Lowell Research Reactor (UMLRR) has recently undergone a series of changes and improvements, including the conversion to low enriched uranium (LEU) fuel in the summer of 2000 and a major instrumentation upgrade in 2001.[1-3] In addition, during this same time period, a new ex-core fast neutron irradiation facility has been designed, constructed, and installed within the pool of the UMLRR. The purpose of this new experimental facility is to provide a large-volume irradiation location that has a high fast neutron flux, with correspondingly low thermal neutron and gamma fluence rates.

The new FNI has a modular design to allow flexibility for future modifications, as needed. It consists of a particular configuration of lead shield blocks, aluminum blocks, the actual irradiation canister, a large Al collar that helps guide the sample canister into position, and a flux-shaping element within a large 11x9 grid arrangement. The modular Pb shield elements have a borated aluminum liner to help minimize the thermal flux in the vicinity of the sample canister. The single flux-shaping element modifies the fast flux distribution so that it is relatively uniform over a 12"x12" area parallel to the side of the core. In addition, samples that attenuate the fast flux by more than 10-20% across the sample thickness will be rotated 180^o at the midpoint of the irradiation period to give a nearly uniform fast fluence throughout the sample. Samples as large as 12"x12"x6" can be easily accommodated -- however, neutronically "thick" sample materials may be limited to a smaller physical thickness if uniformity is a real concern.

The installation of the new ex-core irradiation facility did force some changes to the existing in-core fuel assembly and reflector element configuration. Also, for optimal performance of the FNI, five 3"x3" leaded-void boxes were designed to replace the five in-core graphite reflector elements closest to the new irradiator. In addition, a new arrangement of partial and full LEU fuel elements was needed to counter reactivity effects caused by the composite facility changes. Overall, however, the new facility only required minor changes in the operational characteristics of the UMLRR.

The goals of this paper are to describe the design philosophy and final configuration for the new fast neutron irradiator (FNI) and to present some summary results from a series of 2-D VENTURE[4] and DORT[5] models for the complete facility. In addition, some limited preliminary results from the initial experimental characterization of the new facility are presented and compared to the computational analyses.

II. DESIGN CRITERIA

The ultimate goal of Fast Neutron Irradiator (FNI) project was to design, build, and install a new experimental facility that has a relatively high fast fluence rate with a relatively low thermal neutron and gamma ray background component. The experimental volume should be significantly larger than the existing in-core irradiation canisters, and it must be readily accessible from the pool surface for easy sample manipulation. The facility should be neutronically decoupled from the core so that the FNI sample canister can be loaded or unloaded during power operation with minimal reactivity effects. Finally, the design and operation of the facility should result in a relatively uniform fast fluence distribution throughout the sample. These generic goals were translated into a set of quantitative design specifications. In particular, the new fast neutron irradiator (FNI) was designed

- to accommodate experimental samples as large as 12"x12"x6",
- to have a fast flux $\geq 10^{11}$ n/cm^2-s,
- to minimize the thermal neutron fluence and gamma dose to the sample to the extent possible -- minimal goals here were a 10:1 fast-to-thermal flux ratio and a total gamma dose rate to the sample $\leq$ 100 Krad/hr,
- to achieve a uniform distribution of the fast flux throughout the sample to within $\pm$10% of the average value, and
- to have a maximum reactivity effect that is significantly below the Technical Specification limit for movable experiments in the UMLRR (0.1 %Δk/k).[6]

III. DESCRIPTION OF THE FNI

To meet the above design criteria several trade-offs and iterations upon various design concepts were made. A modular arrangement, including the sample canister, several shield elements, four aluminum blocks, a large Al guide collar, and a single flux-shaping element, all fitting within a large grid structure just to the side of the core, was chosen as the final FNI configuration. The ex-core location was selected for relatively easy access to the large experimental volume and to minimize any influence on core operation during use of the new facility. This choice, however, required the removal of the three existing beam ports on that side of the core. With the beam tubes removed, there is about 3 ft of working space between the pool liner and the side of the core box. The FNI grid, support structure, and the individual modules that make up the complete FNI facility all fit within this space. A conceptual sketch, which highlights the UMLRR core in the center, the three remaining beam ports at the bottom of the figure, the large graphite reflector on the right, and the general location of the new FNI grid and sample canister at the top, is given in Fig. 1. Note that this top view of the complete facility, including some of the existing core structures and piping, hides the first row of the FNI grid. Even so, the rough sketch in Fig. 1 gives a reasonable view of the new facility looking down from the pool surface.

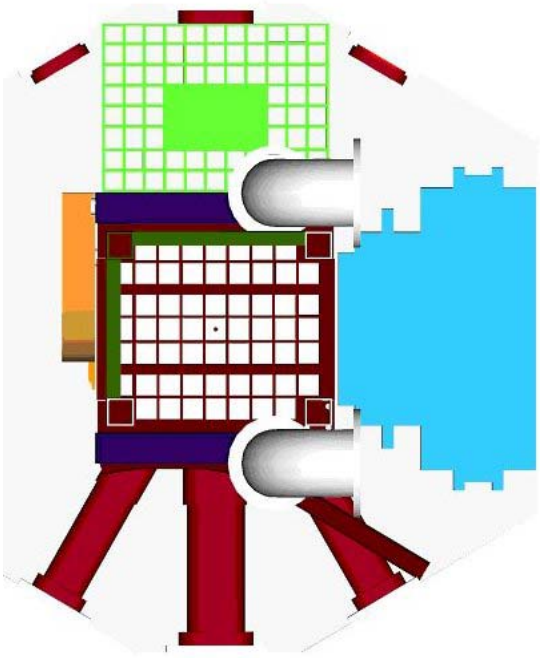

Fig. 1 Conceptual sketch (top view) of the UMLRR with the FNI grid present.

III.A. The FNI Support Structure

The irradiator has been designed to provide a modular system that can be modified to accommodate changes in the irradiation configuration within limited parameters. This flexibility should allow for modifications to the irradiator, as needed, to account for changes to the reactor core configuration over time.

The reactor core grid system is configured on a 3.06" square grid. All elements for the irradiator design continue to use this 3.06" square grid for sizing (though some elements can occupy more than one grid space). This size was utilized for two primary reasons: the first being the availability of handling equipment for elements in this size range, and secondly, the familiarity of the reactor staff to manipulate elements of this size.

The actual support structure is constructed from 6061-T6 aluminum. It contains an 11x9 grid on a 3.06" pitch, a grid support channel, and five circular supports on a conformal base plate. A sketch of this structure, with the FNI sample canister inserted, is given in Fig. 2.

The grid is constructed from aluminum sheet stock. The individual 7/16" plates were spot welded after insertion into the grid configuration. The support channel is fabricated from a 4" aluminum channel welded to the outer perimeter of the grid. This component spreads and uniformly distributes the load from the grid to the support columns. It also serves as a lifting point to lower or transport the physical unit into its location alongside of the reactor core. This was accomplished by four lifting rings welded to the sides of the grid support and the grid, permanently attaching the two components.

The five circular supports are configured to allow for 3-point leveling of the unit to the reactor core. The grid supports are fabricated from 4" schedule 80 (0.337" wall thickness) 6061-T6 pipe. The support columns are threaded into each respective component (conformal base plate and grid support frame), providing a mechanism for positioning and adjusting the irradiator relative to the reactor (threaded supports provide an elevation control mechanism). Pressure release holes are drilled into all the system components that could potentially create voids.

The conformal base plate was statically mounted to the reactor floor without the use of mechanical pinning. The 1100 series aluminum base plate conforms to any irregularities that may be present on the reactor floor. The conformal plate also helps to spread the irradiator load over a wider area.

III.B. The FNI Grid Elements

The FNI grid holds four primary components: lead shielding elements, solid aluminum blocks, a single 3"x9" flux shaping element, and a large dry canister that holds the sample to be irradiated. In addition, a large Al collar sits on top of the assemblies directly surrounding the sample canister to help guide the sample box into position. Each of these elements is described briefly below:

Shielding Blocks: The final FNI design has more than 7 inches of lead shielding between the core and the sample canister, with another 2.4" of lead

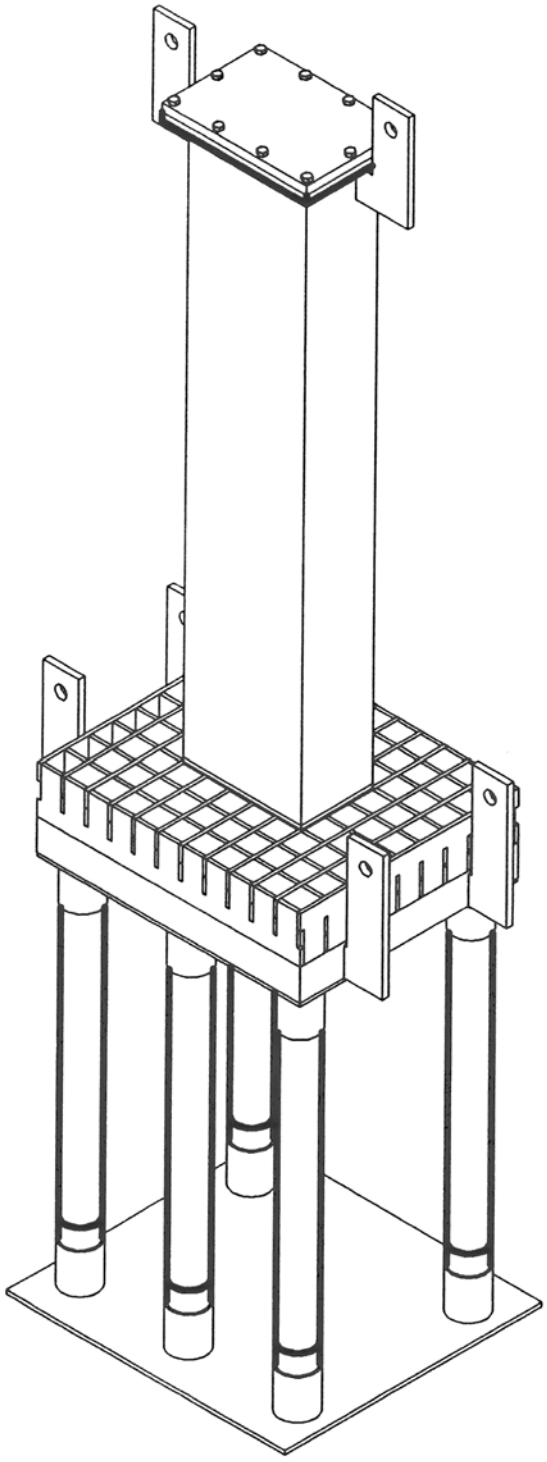

Fig. 2 CAD drawing of the FNI grid and support structure.

on the remaining sides of the sample holder. This gamma shielding is provided primarily in the form of 3”x6” and 3”x9” lead blocks that are designed to fit into the FNI grid structure. The Pb in each block is contained within a 3/16” thick aluminum can that is lined on the inside with a thin sheet of borated aluminum. A small water gap (between 1/16” and 1/8”) is needed for cooling and for ease of insertion and removal of the elements. The approximately 2.4” of lead within each block attenuates the gamma flux from the core and the secondary gammas generated in the water surrounding the FNI grid. The borated aluminum along the inside walls keeps the thermal flux sufficiently low so that secondary gamma generation in the lead is not a problem.

Aluminum Blocks: A series of optimization studies showed that the uniformity of the fast fluence was enhanced if the water just outside the lead blocks along the sample sides is replaced by aluminum. Thus, four 3”x6” solid aluminum elements were used to fill these grid positions. These Al blocks tend to reduce the fast flux gradient just outside the sample region, thereby flattening the fast flux profile within the experimental volume.

Flux Shaping Filter: The only anticipated movement of the sample during an irradiation cycle is a single 180^{o} rotation at the midpoint of the cycle. This single rotation is needed to improve uniformity of the fast fluence through the 6” thick sample. The uniformity in this direction (along the y-axis in all the subsequent models) is directly associated with the attenuation properties of the actual sample material. The 180^{o} rotation tends to mitigate this situation and, for “neutronically thin” samples, a very flat fluence profile can be achieved. However, if a particular material attenuates the fast flux to a large degree, the physical thickness may be limited to less the actual canister size, especially if uniform irradiation is a high priority consideration.

The uniformity constraint in the XZ plane parallel to the side of the core is achieved with a flux-shaping filter. This filter is quite simple and its construction is similar to a standard 3”x9” shielding element, including the aluminum can, borated aluminum internal liners (two 0.1 cm thick B-Al sheets are used in this element), and the central region of high-density lead. The key difference, however, is that a rectangular water-filled “cut-out” is included as part of this element. The water region is positioned to flatten the fast flux peak that is observed in the roughly “cosine-shaped” fast flux distribution. Design calculations indicated that the water region thickness should vary between 1.0” to 1.5”, and that it should be about 12” long and nearly 5” wide in the z and x directions, respectively. The water cut-out within the standard shielding block is slightly off center because the core flux distribution is asymmetrical along the x and z axes. In particular, the rough cosine-shape is shifted towards the graphite thermal column in the x-direction and the axial flux profile is bottom peaked because the control blades are always partially inserted into the core. The final design for the water cut-out region is highlighted in Fig. 3, which shows a photo of the actual flux-shaping element along side an in-core Pb-void box (see below). This filter concept is really quite simple and quite effective in flattening the fast flux distribution over the desired 12”x12” sample area parallel to the core face.

Fig. 3 Photo of 3”x9” flux-shaping element along side an in-core Pb-void box.

Sample Canister: The sample to be irradiated will be housed in a large dry canister that occupies 15 positions within the FNI grid (a 5x3 grid region). The canister outer dimensions are about 15”x9”x60”. The large height will facilitate early removal of the samples by keeping the relatively high activity aluminum structures below the

surface of the pool. The bottom of the canister has about 4" of lead to offset the buoyancy forces associated with the displaced water and to provide additional gamma shielding along the bottom surface. A holding rack, placed just above the lead within the canister, centers the sample about 2" below the centerline of the core to achieve the maximum fluence rate. Thin borated aluminum sheets line the inside walls of the canister to reduce the thermal flux seen by the sample. The top of the canister is a simple cover and gasket arrangement with several bolts to keep the container water free. Two lifting rings are an integral part of the cover/upper canister design to allow the single 180^{o} rotation at mid irradiation and to bring the canister to the pool surface for insertion and removal of the samples. A sketch of the sample canister is given in Fig. 2 and a photo of the as-built unit is shown in Fig. 4.

Fig. 4 Photo of large sample canister.

Aluminum Guide Collar: As in the XY plane, design calculations showed that removing some additional water near the top of the sample region tends to gives a slightly better axial fast flux profile. To accomplish this and to provide a guide for easy insertion of the sample canister, a 3" thick aluminum collar is positioned over the shield blocks directly surrounding the sample region. The top of the collar is slanted inward, with the height varying from 8" on the inside to 12" on the outside. A 1.5" thick by 5" high cut-out was made on the top core-facing side of the collar to allow room for some of the core piping structures when the reactor bridge and core are in their normal operating position.

A series of three photos, given in Figs. 5-7, provide a good summary view of the FNI support structure and the modular components the make up the FNI facility. These figures show the facility during various stages of the installation process. Figures 5 and 6 show illustrative side and top views, and they give a good perspective of the facility placement within the reactor pool. Figure 7 shows the final configuration of the modular elements within the grid, and it highlights the Al guide collar (before the cut-out was made on the front face) and the opening for the sample canister.

Fig. 5 Side view of FNI during installation.

Fig. 6 Top view of FNI during installation.

Fig. 7 FNI configuration with Al collar.

These three pictures, together with the above description, provide a reasonable overview of the physical construction of the new ex-core fast neutron irradiation facility installed within the UMLRR.

III.C. In-Core Modifications

The installation of the new ex-core experimental facility also required a number of changes to be made to the in-core configuration. A sketch of the pre-FNI LEU core configuration is given in Fig. 8. This core configuration was identified by the operations staff at the UMLRR as the M-1-4 core. Of particular interest are the graphite reflector elements in row A (next to the three beam ports in the top part of the sketch). Recall that the beam tubes on this side of the core were removed to make room for the new FNI facility. Since one of the primary objectives of the FNI design was a high fast neutron flux in the sample region, it was very clear early in the design study that several of the graphite elements had to be removed – they simply caused too much attenuation of the fast flux! This decision, however, led to the dilemma of what to put in place of the graphite reflectors, since water attenuates the fast flux even more than the graphite.

After several iterations, a new in-core element was designed that contains about 0.5 inches of lead on either side of an air space. This new in-core element is referred to as a lead-void box. It is about 29" long with a 3"x3" square base so that it fits into a standard core grid position. Five of these elements (see Fig. 3) were fabricated and inserted into the central five positions of row A within the core grid. This design feature provides about 1" of primary gamma shielding and it also tends to neutronically de-couple the core region from the remainder of the FNI facility. More importantly from the FNI perspective, however, is that these elements do not significantly decrease the fast flux.

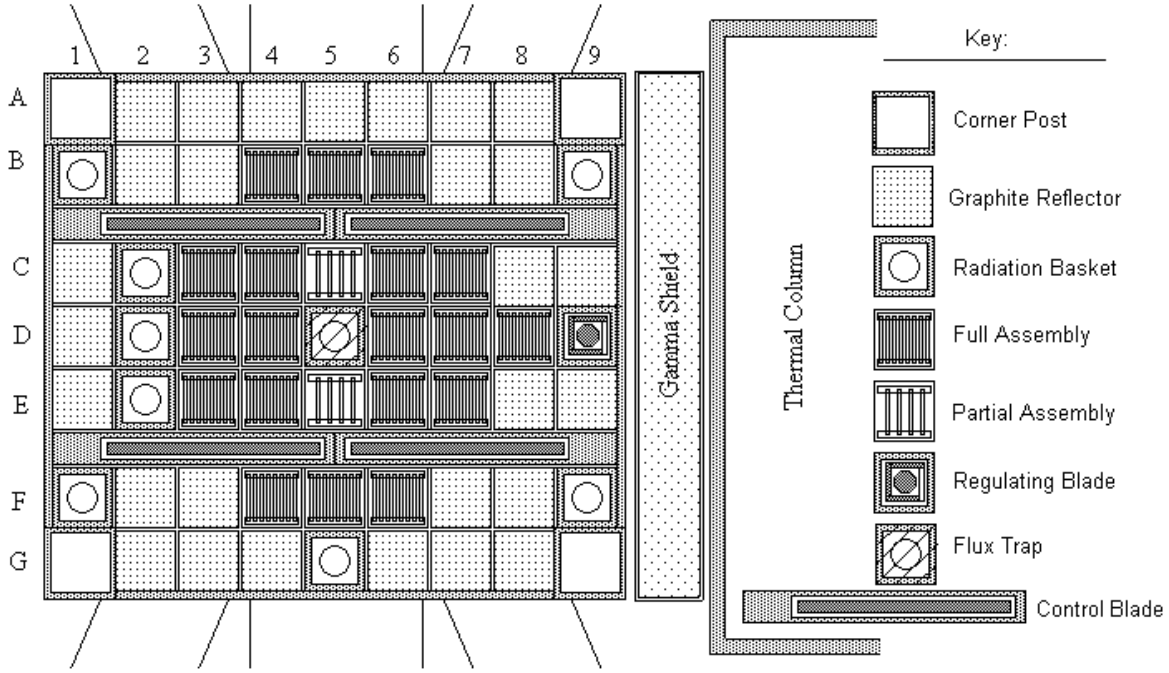

Fig. 8 Core layout for the pre-FNI M-1-4 configuration.

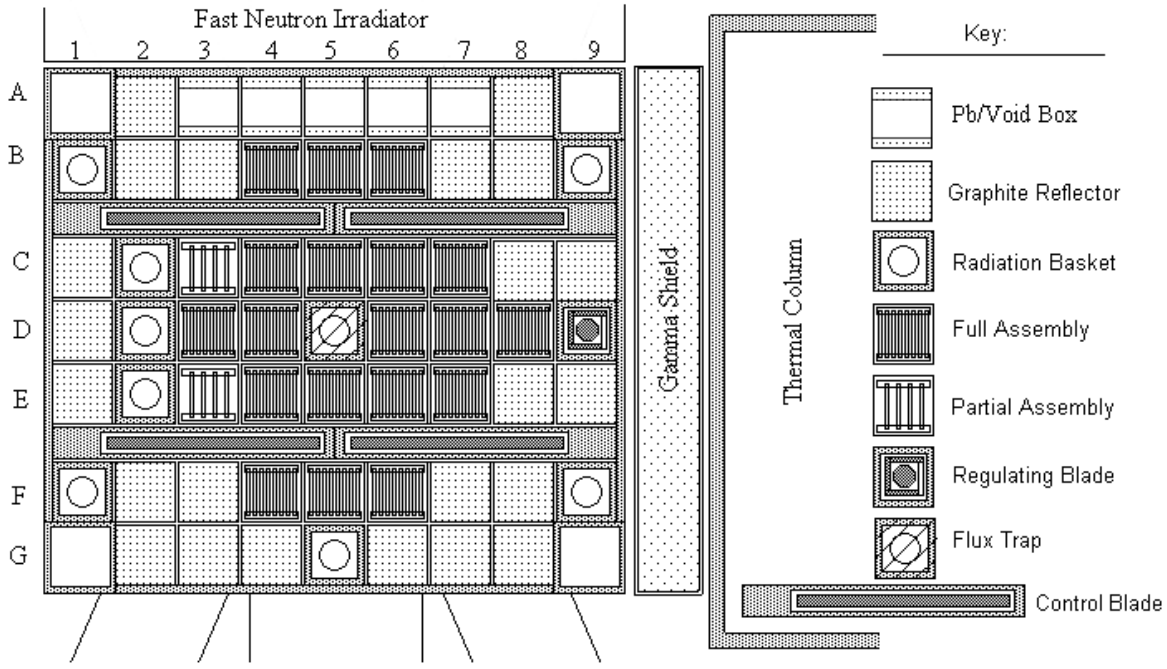

Fig. 9 Core layout with the FNI facility installed (M-2-5 configuration).

The replacement of five graphite reflectors with Pb-void boxes also caused a fairly substantial decrease in core reactivity. This was offset by interchanging the two partial fuel elements in positions C5 and E5 with the full fuel assemblies in C3 and E3. Moving these two full assemblies into a higher-worth region was just enough to counter the negative reactivity introduced by the five Pb-void boxes. These composite changes also cause a shift in the in-core flux distribution and control blade worth distribution towards the lower right part of the core (relative to the diagrams in Figs. 8-9).

The result of the in-core modifications identified above is shown in Fig. 9. This core configuration, denoted as M-2-5, represents the post-FNI layout, and it is now being used in routine operation of the UMLRR.

IV. DESIGN CALCULATIONS AND RESULTS

The installation of the new ex-core irradiator and the resulting changes to the in-core configuration represent a major modification to the pre-FNI UMLRR facility. To justify these changes and as primary support for the design optimization process, a series of reactor physics computations were performed using both XY and YZ models within the VENTURE and DORT codes. This section of the paper first overviews the basic methodology used at UMass-Lowell to perform these analyses, and then it summarizes the actual models and results of the VENTURE and DORT calculations. These summary results support the many design choices made during the course of this project, and they show that the design criteria listed in Section II are indeed satisfied by the final FNI design.

IV.A Computational Methodology

Our traditional approach to deterministic reactor physics modeling at UMass-Lowell involves heavy reliance on the VENTURE and DORT codes.[4-5] VENTURE is used to do few-group diffusion theory calculations for the core region and its immediate surroundings, and DORT is utilized to perform multigroup transport computations for the determination of in-core neutron and gamma spectra and for all ex-core radiation transport analyses. The VENTURE and DORT modeling steps are highly-coupled via a series of in-house Matlab codes that assist in the model-building process, in the conversion of the VENTURE-calculated fission source to a DORT input distributed source, and in the post-processing of results from both codes (see Refs. 2 and 3 for further details on the Plot_Vgeo, Plot_Vpwd, and Plot_Flux codes). In short, VENTURE is used to address core operations (reactivity worths, power distributions, etc.) and DORT is used to quantify

the space and spectral distribution of the neutron and gamma radiation environments within the various experimental facilities in the UMLRR.

With the change to LEU fuel in the summer of 2000, a significant effort was made to update existing models of the reactor and to generate new LEU-specific cross section libraries for future analyses.[2-3] In particular, consistent sets of DORT and VENTURE cross sections were developed specifically for the LEU core using several modules of the SCALE system[7] and the base VITAMIN-B6 library.[8] The original 199/42-group energy structure in VITAMIN-B6 was collapsed to 47 neutron groups and to 20 gamma groups for the DORT calculations and to a simple 2-group neutron library for use in the VENTURE eigenvalue calculations. The coupled 67-group DORT library is fully compatible with the energy structure from the BUGLE-96 library[9] and many of the response functions from the BUGLE-96 distribution were used as part of the analyses performed here. The reader is referred to Ref. 2 for further details on the cross-section generation procedure.

IV.B XY and YZ Modeling Considerations

Putting together a computational model of any reactor system is always challenging. For the current work, a set of XY and YZ 2-D models is used to approximate the behavior of the real 3-D core and FNI geometry. As such, a number of approximations are required to make the 3-D to 2-D transition.

In general, the UMLRR XY models for both VENTURE and DORT are quite representative of the actual planar geometry near the central plane of the core in the axial direction. The core region is naturally broken into its actual 9x7 grid-like structure and, since the new FNI also has an 11x9 grid arrangement of identical pitch, the same zone representation is used in both regions. Within a grid position, the geometry is broken in three (or more) regions, consisting of the central region, edge zones, and side zones. Inside of these regions, the actual heterogeneous geometry is homogenized for computational modeling purposes. A consistent set of homogenized material compositions are then generated for use within the homogenized zones using a material-by-zone mapping arrangement. This procedure is quite traditional and, with a little care and a little experience with this basic methodology, very representative results from the computer modeling can be expected.

The result from the XY modeling step is illustrated in Fig. 10, where the first part of the figure shows the full XY model and the lower half displays an expanded view of the important core and FNI regions (these figures were generated with the Plot_Vgeo code). The homogenized regions mentioned above can be clearly identified, along with many of the explicit structures within the core (fuel elements, control blades, leaded-void boxes, etc.), previous experimental facilities (thermal column, the three remaining beam ports, etc.), and the new ex-core FNI facility (shield blocks, pure aluminum elements, the flux-shaping element, and the sample and canister regions). The actual model contains over 950 zones and a relatively fine mesh with a 181x231 mesh grid in the x and y directions, respectively. Note that the base XY model does not have any control inserted.

A similar effort was made to generate a representative YZ model of the post-FNI UMLRR facility. The choices here, however, are greater, since it is not clear which x location to choose for the YZ planar model. Since a direct cut through the center of the core is not really representative (because of the central flux trap in location D5 and source holder in position G5), a YZ cut just to the right of the central assembly was chosen. This too has its faults, since no other x location has exactly the same material profile along the y-axis. This dilemma is a direct result of a 2-D modeling methodology applied to an inherently 3-D system. However, even with these inherent limitations, we expect the selected YZ model to give reasonable qualitative results that are sufficient for general design and analysis purposes.

The resultant YZ computational model is shown in Fig. 11, where again, the full model is displayed in the upper half of the figure and an expanded view of the core and FNI regions is highlighted in the lower diagram. This model shows explicit zones for the fuel elements, control channels, Pb-void box, shield blocks, flux-shaping filter, and sample canister. In addition, the treatment of the axial direction allows the representation of the upper and lower reflectors, the FNI and core grid boxes, the aluminum guide collar, the full extent of the sample canister, and even several explicit zones to model partially inserted control blades. This model contains over 250 zones and has a fine mesh structure with 231x222 nodes in the y and z directions, respectively. The y-direction mesh is identical for the XY and YZ models. All the YZ model results given here have the blades at 15” withdrawn (as illustrated in Fig. 11).

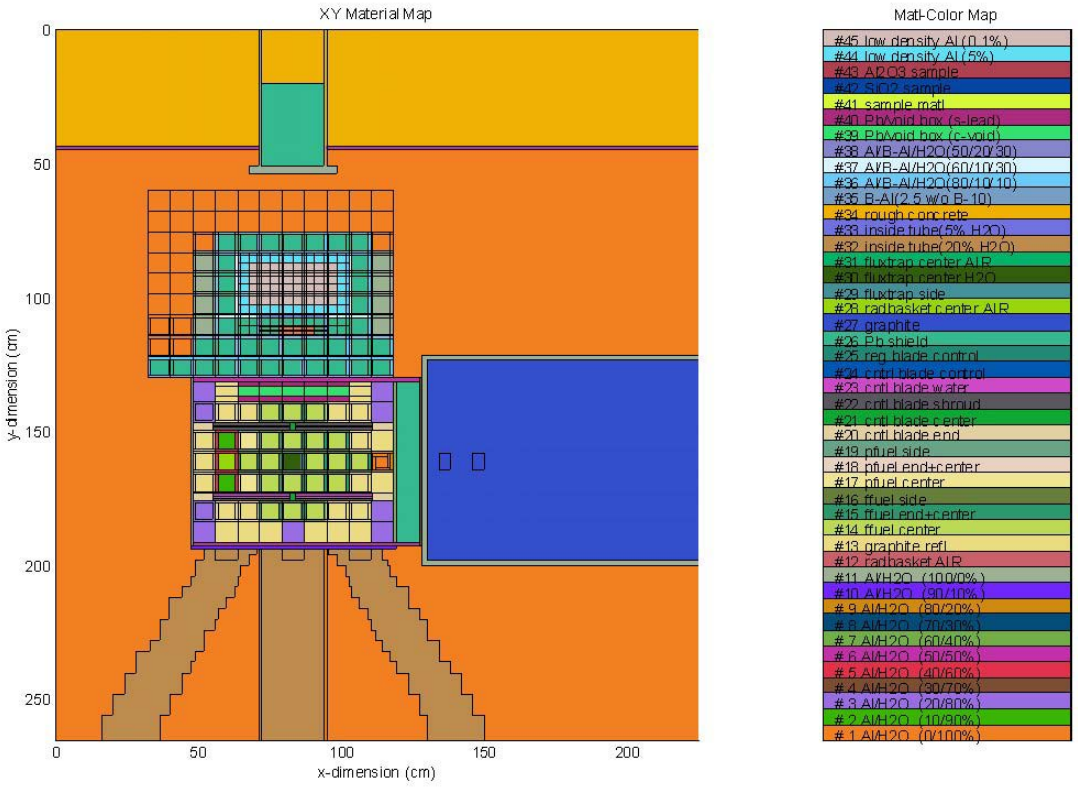

Fig. 10a Full view of XY computational model.

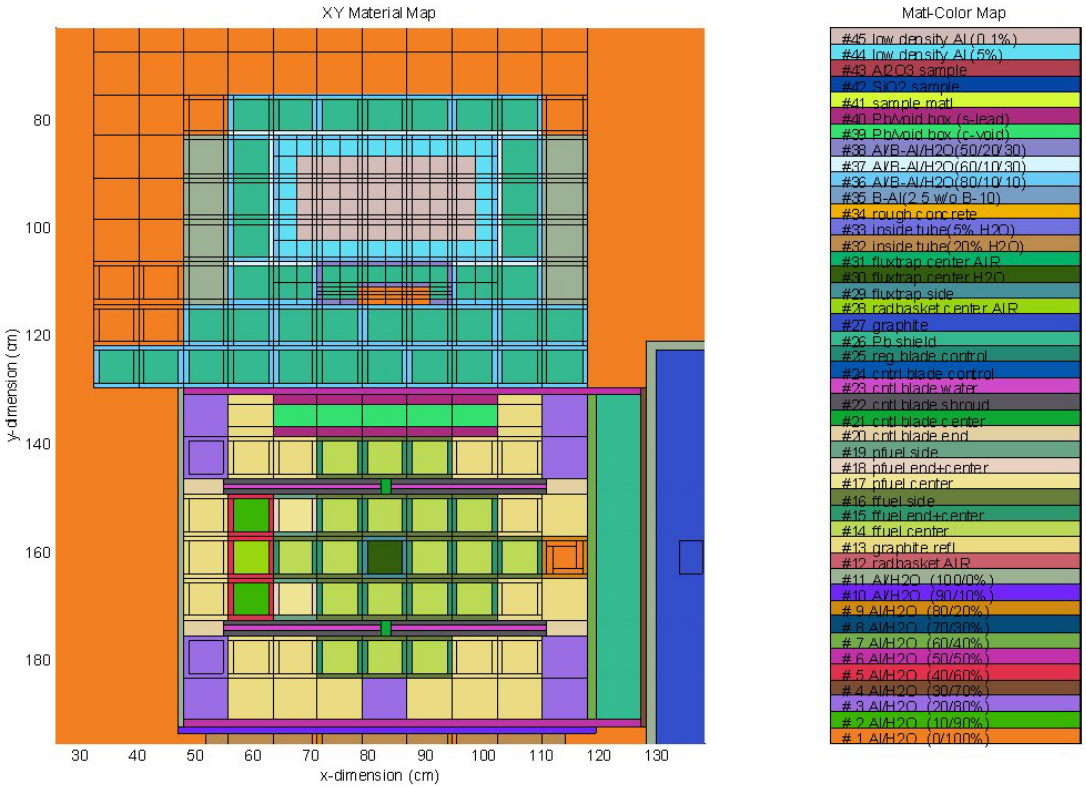

Fig. 10b Expanded view of core and FNI from XY computational model.

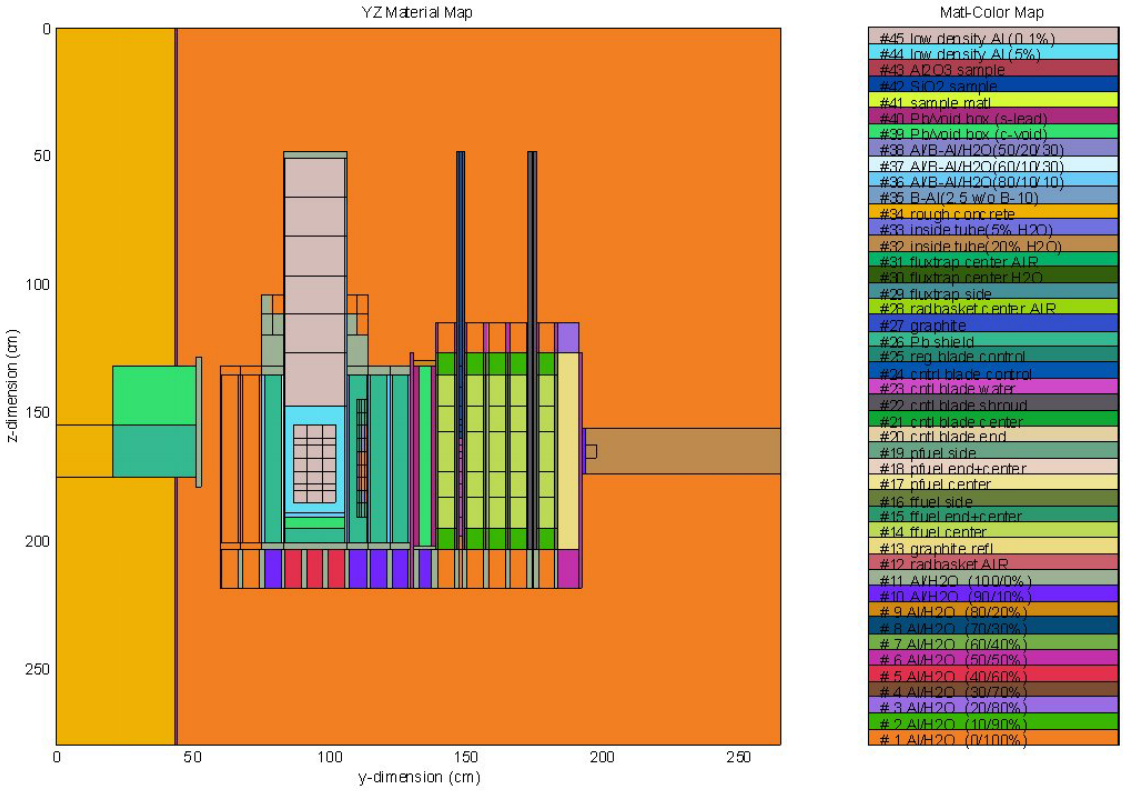

Fig. 11a Full view of YZ computational model.

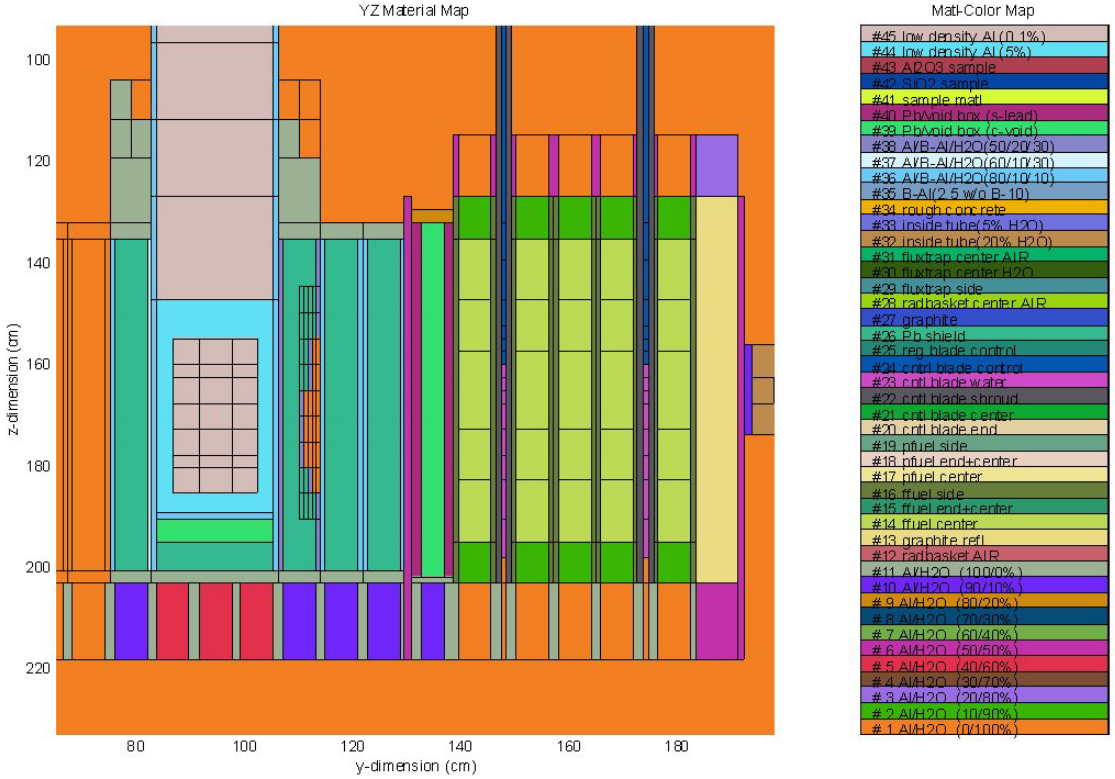

Fig. 11b Expanded view of core and FNI from YZ computational model.

IV.C Core Operation and Safety

To support operation of the new M-2-5 core configuration with the FNI present, a series of blade worth predictions was made using the 2-D XY VENTURE model shown in Fig. 10. Summary data from these calculations are given in Table 1 along with similar computational results from the pre-FNI M-1-4 model. Note that the blades are numbered 1 through 4 in a clockwise fashion starting with the lower left blade in the XY model. Thus one can see a clear shift in the blade worth distribution for the M-2-5 layout, with Blades 1 and 4 having more worth than Blades 2 and 3. This shift was expected because the addition of the five Pb-void assemblies in the A3-A7 grid locations causes the flux to tilt towards the lower portion of the core region as sketched in Figs. 8-10. In addition, the movement of the partial fuel assemblies to the left side of the model will cause the flux to be skewed a little more to the right side, making Blade 4 the most reactive blade -- and this is what is observed in Table 1.

Table 1. VENTURE-calculated reactivity data for the M-1-4 and M-2-5 models

Parameter	M-1-4 %Δk/k	M-2-5 %Δk/k
Excess Reactivity	4.33	4.19
Blade 1 Worth	2.67	2.87
Blade 2 Worth	2.74	2.14
Blade 3 Worth	3.44	2.99
Blade 4 Worth	3.67	3.96
Sum Blades 1 - 4	12.52	11.96
Min. Shutdown Margin*	3.87	3.16

* This conservatively assumes that the most reactive blade is stuck out of the core, that +0.5 %Δk/k is added due to movable experiments, and that another +0.15 %Δk/k is added due to the flooding of a single beam tube.

Note also that the minimum shutdown margin decreases slightly because of the lower total worth and the stuck blade assumption. However, this quantity is still above the Technical Specification limit of 2.7 %Δk/k.[6] In addition, our experience to date has shown that the VENTURE models tend to over-predict the initial excess reactivity relative to measured data. Thus, it is expected that the real shutdown margin will be somewhat greater that the value listed here.

It should be emphasized that the non-symmetrical worth distribution and the lower shutdown margin for the post-FNI system relative to the pre-FNI configuration are not a real concern. The shutdown margin still exceeds the pre-defined limit, and the UMLRR has been operated safely for over 25 years with an asymmetrical distribution along the x-direction (i.e. the worth of Blades 1 and 2 have always been much lower than the worth of Blades 3 and 4). Thus, a slight additional tilting towards Blade 4 does not appear to be a real concern.

A series of safety analyses was also made to address the operational safety of the new post-FNI core configuration. Only three issues could be identified that might affect the reactivity level or flux distribution within the system. These are discussed briefly as follows:

1. Power/Flux Peaking due to Pb-Void Elements: The peak power density in the core is expected to increase slightly due to the flux tilting caused by the asymmetric placement of the five Pb-void elements and the movement of the partial fuel assemblies. Comparing this quantity from the two VENTURE models shows an increase of about 4% in the peak power density in the new configuration relative to the reference core. This change is quite small and it will not have any impact on the safety analyses performed for the UMLRR with LEU fuel (note that a 10% power density uncertainty was included in the original safety calculations).[1]

2. Reactivity Effect due to Flooding of a Single Pb-Void Element: The design of the Pb-void elements includes an air gap between layers of lead canned in aluminum. A credible accident scenario needs to include the reactivity addition associated with an instantaneous flooding of the most reactive of these elements. In particular, the void region in the element in grid position A5 was filled with water and the resulting reactivity worth was computed to be only about 0.20 %Δk/k. This is well below the 0.50 %Δk/k step change included as part of the original safety analysis.[1] Thus, a sudden leak in one of these new elements poses no serious safety concern.

3. Reactivity Effect due to Movable Experiments in the New FNI: The sample canister associated with the new FNI facility is located in the ex-core region with more than 7 inches of lead shield between the core and the large-volume experimental location. The Technical Specification limit on movable experiments is 0.1 %Δk/k for each experiment.[1] However, the VENTURE calculations for cases with and without the sample canister present in the facility showed only a

negligible effect on reactivity (less than 0.01 %Δk/k). Thus, we cannot envision any situation where normal use of the new experimental facility during power operation will have any significant effect on the core reactivity.

Based on the above VENTURE computations, it appears that normal operation of the reactor should not be adversely affected by the changes associated with the new ex-core FNI. Since the new configuration satisfied all operational and safety concerns, it has now become the nominal configuration for routine operation of the UMLRR.

IV.D FNI Design Considerations

Certainly one aspect of designing a fast neutron irradiator is the removal of the undesirable components of the radiation field -- in this case, the thermal neutron and gamma fluxes. In the current design, using more than 7" of lead shielding between the core and sample area minimized the gamma dose due to core gammas. In addition, nearly 2.5" of lead was also placed completely around the sample canister to reduce the dose due to secondary gammas produced in the water outside the FNI modules.

However, even with this amount of lead in the model, the total gamma dose to the sample exceeded our original design limits. Upon further study, we found that there was a significant amount of secondary gamma generation directly in the lead itself. To remove this dose component, a borated aluminum liner was placed in each of the shield blocks. This poison liner significantly reduced the thermal fluxes throughout the FNI facility, which also reduced the secondary gamma generation in the lead to acceptable levels.

Once the gamma dose limit had been met, achieving the pre-set minimum fast-to-thermal flux ratio was quite easy, since the poisoned shield blocks already significantly reduced the thermal flux. However, just to minimize the thermal neutron levels to the fullest, an additional borated aluminum liner was also placed directly inside the sample canister. This gives an extra layer of thermal neutron attenuation at the sample location, and it quite effectively removes most of the remaining thermal neutrons produced in the water-filled flux-shaping region just in front of the sample canister.

Figure 12 illustrates the effectiveness of the various layers of lead and borated aluminum within the FNI components. This plot shows the y-directed distribution of the fast and thermal neutron fluxes and the total gamma flux. The flux data are from the XY DORT model just to the right of the core centerline. For clarity, the locations of the sample region and the fueled portion of the core have been annotated on the plot.

As apparent in Fig. 12, the fast and thermal neutron fluxes in the core region are on the order of 10^{13} n/cm^2-s and the total gamma flux exceeds $5x10^{13}$ γ/cm^2-s. Just outside the fuel, the Pb-void elements cause a sharp drop in the gamma flux, without significant attenuation of the neutron levels. In the first two rows of shield elements (about 115 cm to 130 cm in the plot), however, there is significant attenuation in both the gamma flux level and the thermal neutron component of the radiation field, yet the fast neutron component remains relatively high in this region. The impact of the water associated with the flux-shaping element at about 110 cm is also apparent, with a large peak in both the thermal flux and gamma flux and a factor of 2-3 drop in the fast flux. Finally, the effectiveness of the last layer of lead and borated aluminum liner directly surrounding the sample canister is also apparent, with another decrease in the gamma and thermal neutron fields. From the data in Fig. 12, it is clear that the composite FNI design gives the desired large fast neutron flux within the sample, with correspondingly low gamma and thermal neutron background levels. And, with a fast flux of nearly $2x10^{11}$ n/cm^2-s in the sample region, this design meets the original 10^{11} n/cm^2-s criterion for the ϕ > 0.1 MeV flux.

Once the proper sample flux levels were achieved, the only remaining concern was associated with the spatial distribution of the fast flux within the sample volume. Recall that the pre-defined uniformity constraint required that the fast flux throughout the sample be within $\pm$10% of the average value. This design specification was met in the y direction by allowing the sample canister to be rotated 180^o at the midpoint of the irradiation cycle and by limiting the thickness of samples with large fast neutron attenuation cross sections. In the XZ plane, however, controlling the fast flux distribution was more challenging, and this led to the design of the flux-shaping element discussed in Section III.B.

As seen in Fig. 3 and in the model material maps in Figs. 10-11, the "shaping" effect in the flux-shaping assembly is simply due to the water that is associated with this assembly. The impact of

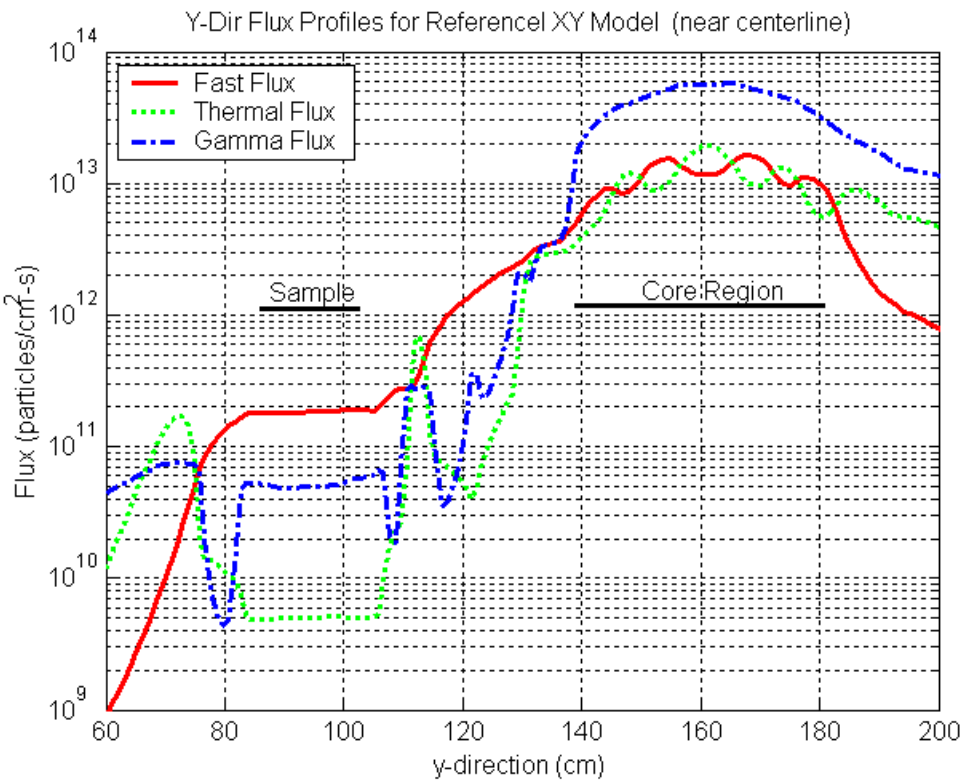

Fig. 12 Y-directed flux profiles from the DORT XY model.

the water in this element is certainly apparent in the y-directed flux profiles shown in Fig. 12. However, it is the final placement and size of the water "cut-out" in the XZ plane and the thickness of each water section in the y-direction that impacts the fast flux distribution. The final choice for these design variables was made after careful analysis of many different configurations in both the XY and YZ DORT models (see Section III.B for a brief description of the final design of the flux-shaping assembly).

As a demonstration of the flux flattening capability associated with an appropriately placed thin layer of water, the flux profiles just before and just after the flux-shaping filter have been extracted from the DORT model results and plotted in Figs. 13-14. The x-directed flux profiles, before and after filtering, are given in Fig. 13a (before) and Fig. 13b (after). Similarly, the z-directed flux profiles before and after the water filter are given in Figs. 14a and 14b. Note that the "just after" profiles are inside the sample canister liner and, therefore, the thermal flux profiles are also affected by the borated aluminum in this region.

As apparent from the "before" and "after" profiles, the water regions within the flux shaping filter were positioned to flatten the fast flux peak that occurs in the "before" x-directed and z-directed distributions. In both the x and z directions, the peak in the roughly cosine-shaped distribution is "cut-off" by the additional fast neutron attenuation in the thin water layers of the flux shaping element. In both cases, the maximum-to-minimum ratio in the fast flux over the sample region is reduced from greater than 1.25 in the "before" profile to about 1.15 or less in the "after" distribution. This indicator, plus the obvious flattening trend observed in Figs. 13 and 14, shows that the final design of the flux shaping element was indeed successful in achieving its intended goal.

IV.E Characterization of the FNI Sample Region

The above discussions have described the new ex-core irradiator, outlined the analysis methods used, and explained "why we did what we did" relative to the design of the flux shaping filter, the shield elements, the in-core Pb-void elements, etc.. Thus, the only item remaining is the actual characterization of the experimental volume, and this subject is treated in detail in this subsection.

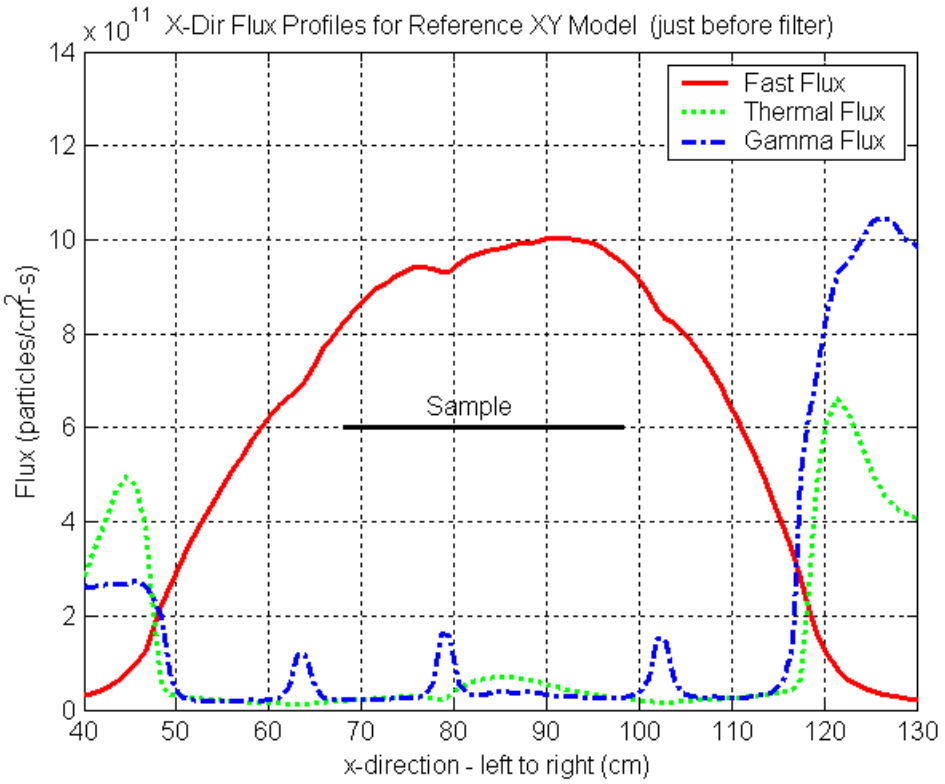

Fig. 13a X-directed flux profiles before the flux filter in the DORT XY model.

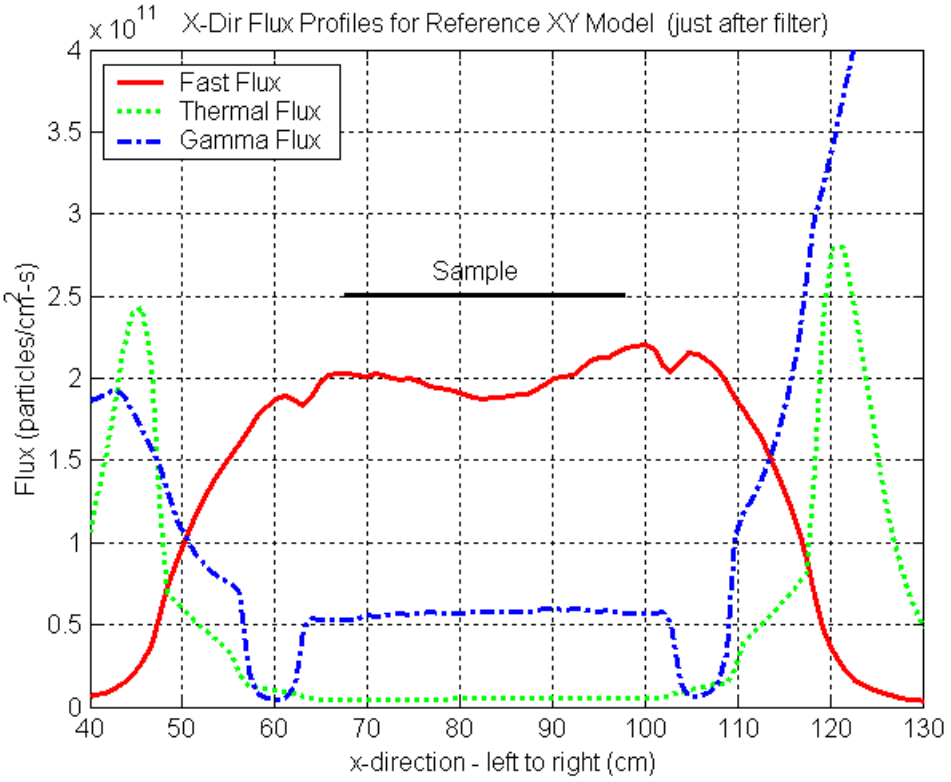

Fig. 13b X-directed flux profiles after the flux filter in the DORT XY model.

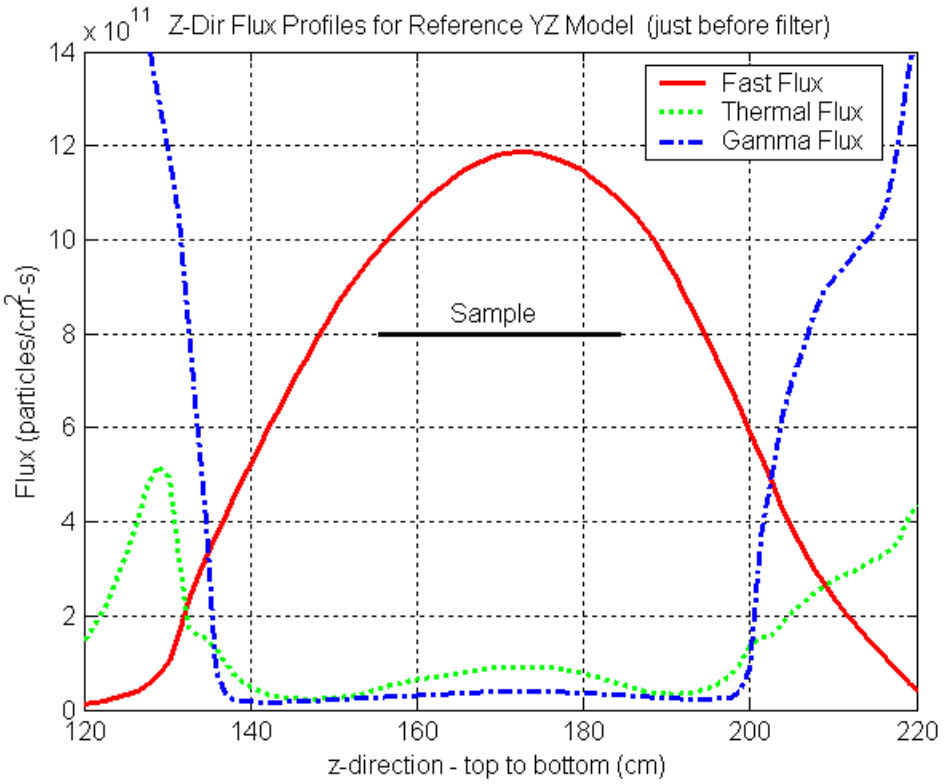

Fig. 14a Z-directed flux profiles before the flux filter in the DORT YZ model.

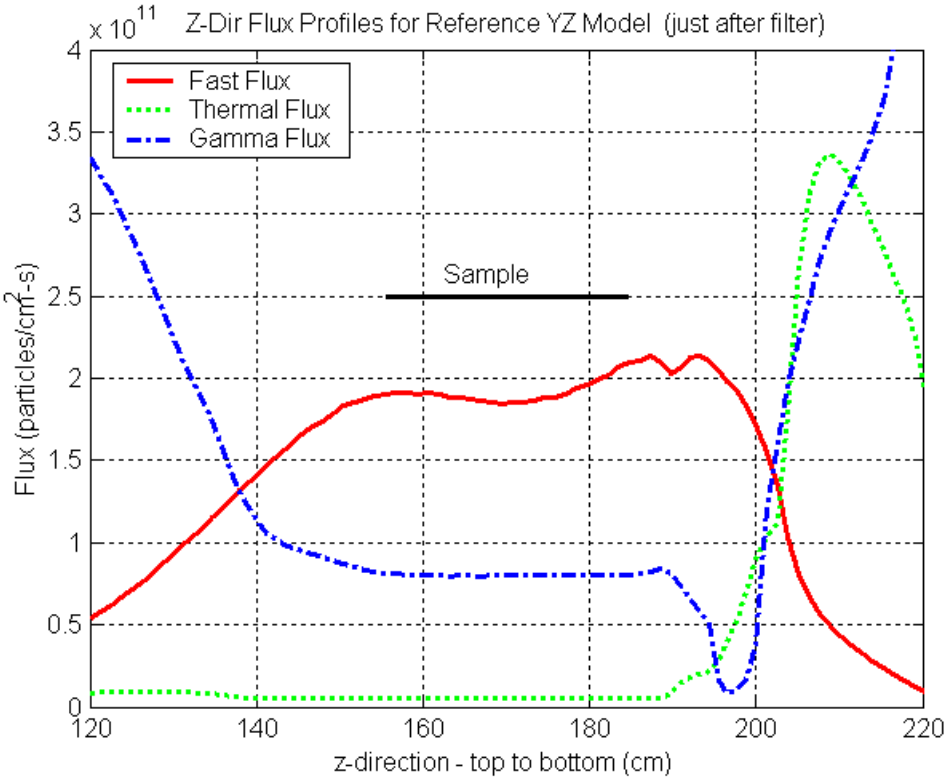

Fig. 14b Z-directed flux profiles after the flux filter in the DORT YZ model.

There are a number of ways to present information relative to the radiation environment observed in a given experimental facility. In particular, 2-D color contour plots are often used to present a big-picture qualitative view of the spatial or spectral distribution of selected quantities. More traditional one-dimensional space-dependent or energy-dependent profiles at selected locations are also frequently used to show the same kind of information. These tend to be generally more useful for quantitative analyses, since the plots are easier to interpret and they allow one to easily extract numerical values as needed. And, of course, integral measures that are representative of the average behavior over a given region are the most frequently used measures of expected performance. The integral data are especially important because they are easy to use and they present a single quantitative indicator of the expected behavior of the given facility.

For the new FNI facility, we provide a combination of all these performance indicators. In addition, some comparisons are made with similar indicators for the radiation basket facility in core position D2. There is a lot of experience with the use of this in-core location, and showing the change associated with a standard in-core irradiation position and the ex-core fast neutron irradiator should be useful in planning new experiments within the new FNI facility.

In addition to the various techniques for presenting the data, there are also many different ways to characterize the neutron spectrum in a particular location. At UMass-Lowell, the DORT 67-group flux information is usually integrated over energy to give four broad-group fluxes (three neutron groups and one gamma group). For the neutron data, the fast group includes neutrons above 0.1 MeV, the thermal group covers energies below 1.0 eV, and the epithermal group includes all energies between these limits. The single gamma group represents an integral over all 20 gamma groups within the base 67-group library structure. Thus, the ϕ > 0.1 MeV is usually used as a measure of the "fast flux" in the system (for example, Figs. 12-14 use this measure of the fast flux).

Additional measures of the fast component of the neutron spectrum are also useful. For example, many researchers are interested in the neutron fluence above 1 MeV, while others include all neutrons above 0.01 MeV. In addition, because of the historical use of the UMLRR facility for irradiation of electronic components, it is also important to quantify the so-called 1 MeV equivalent flux for silicon displacement in the various experimental locations of the UMLRR. The 1 MeV equivalent flux for silicon displacement is formally defined[10] as

$$\phi_{eq}(E_o) = \frac{\int_{E_{min}}^{E_{max}} K_D(E)\phi(E)dE}{K_D(E_o)} \qquad (1)$$

where $K_D(E)$ is the neutron displacement kerma for silicon as a function of energy, E_o is the reference energy of interest, and E_{min} and E_{max} specify the energy range for significant atomic displacement in silicon. Reference 10 suggests the use of 0.01 MeV and 18 MeV as limits for the energy range of interest and E_o is usually 1 MeV. The suggested value for the displacement kerma at 1 MeV is 95,000 eV-b, and this is used as $K_D(E_o)$ in eqn. (1). The energy-dependent kermas used in this study were obtained from the BUGLE-96 library,[9] since the 47-group neutron energy structure in BUGLE-96 is identical to the energy bins chosen for this study.

Reference 10 also defines the "neutron energy spectrum hardness parameter" or simply the relative damage factor (RDF). The RDF is given by

$$RDF = \frac{\int_{E_{min}}^{E_{max}} K_D(E)\phi(E)dE}{K_D(E_o)\int_{E_{min}}^{E_{max}} \phi(E)dE} = \frac{\phi_{eq}(E_o)}{\phi_T} \qquad (2)$$

where ϕ_T is the total energy-integrated flux over the interval of interest. The RDF is a convenient measure for characterizing the spectrum of a particular facility. It represents the fluence of 1 MeV neutrons required to produce the same displacement kerma in silicon as a unit fluence of neutrons of spectral distribution $\phi(E)$.

As a final indicator of the radiation environment, the energy deposition rate in air and silicon, as well as other materials, are also usually tabulated for the different experimental facilities within the UMLRR. These data are useful as qualitative and quantitative measures of the expected neutron and gamma dose rates in the various facilities. For a particular experiment, material-specific kermas would be needed to determine the energy deposition in a specific sample. However, the relative comparison of typical materials (like air and silicon) give a good indication of how the relative neutron and gamma dose rates vary for the different experimental facilities.

The broad group fluxes, some additional fast flux indicators, and the neutron and gamma dose rates in air and silicon for the D2 in-core position and for the 12"x12"x6" sample volume in the ex-core FNI are summarized in Table 2. These data were determined using the calculated space and energy-dependent flux distributions from the DORT XY model. Note that the calculated in-core data have been multiplied by an axial peaking factor of 1.4 to account for the axial flux profile in the core (see Ref. 3). Thus, these values should be representative of the peak flux locations where the samples are typically irradiated. The ex-core flux and dose values, however, are not normalized in this fashion, since the axial profile in the ex-core regions is expected to be much flatter than in the core region. This approach is very approximate, of course, but lacking full 3-D flux data, this was the procedure adopted in the current work.

As seen in Table 2, the ex-core FNI region has significantly reduced flux levels relative to the in-core radiation basket position. However, also clearly apparent is the fact that the thermal neutron flux and the gamma fluence and energy deposition rates are reduced to a much greater extent relative to the fast neutron component of the radiation field. For example, the 1 MeV flux is only reduced from 3.1×10^{12} to 1.4×10^{11} n/cm^2-s (a factor of about 20-25), whereas the thermal neutron flux and the gamma dose rates are reduced by factors of nearly 2300 and 800, respectively. Thus, it appears that the ex-core irradiator design was indeed successful in significantly reducing the unwanted components of the radiation field, while still maintaining a relatively large fast neutron fluence rate. In particular, Table 2 shows that the original design criteria specified for the FNI facility (see Section II) have been satisfied, as follows:

- the fast flux > 0.1 MeV and the 1 MeV equivalent flux both exceed the design value of 10^{11} n/cm^2-s,
- the minimum 10:1 fast-to-thermal flux ratio is easily met, and
- the gamma dose rates in air and silicon are well below the 100 Krad/hr design limit.

One parameter from Table 2 that requires a little more discussion is the relative damage factor (RDF). An RDF of 0.55 for the FNI facility relative to 0.77 for the in-core radiation position indicates that the high-energy neutron spectrum has been shifted downward in energy. With careful observation, this shift can be seen in Fig.15a, where the energy-dependent neutron flux averaged over the two experimental facilities are compared. This figure, however, really highlights the difference in the thermal component, showing a dramatic difference for the in-core D2 position relative to the FNI location, with a significantly softer spectrum for the in-core location.

Table 2. Integral parameters for in-core location D2 and the new ex-core FNI facility

Parameter of Interest	Radiation Basket D2	FNI Sample
Broad Group Fluxes (n/cm^2-sec)		
Fast Flux >0.1 MeV	3.26E+12	1.83E+11
Epithermal Flux	3.42E+12	2.45E+11
Thermal Flux <1 eV	1.14E+13	4.85E+09
Total Neutron Flux	1.81E+13	4.33E+11
Total Gamma Flux	2.95E+13	5.05E+10
Additional Fast Flux Characterization		
Fast Flux >1 MeV	1.72E+12	5.08E+10
Fast Flux >0.01 MeV	4.02E+12	2.55E+11
1 MeV Equiv. Flux	3.08E+12	1.39E+11
RDF	0.77	0.55
Energy Deposition Rates (Krad/hr)		
Neutrons in Air	2.58E+04	1.38E+02
Neutrons in Silicon	9.37E+02	3.20E+01
Gammas in Air	3.50E+04	4.40E+01
Gammas in Silicon	3.74E+04	4.62E+01

However, if one focuses on only the > 0.01 MeV region, a different picture becomes clear. In particular, Fig. 15b shows the spectra for the > 0.01 MeV flux, where the total fluxes have been normalized to unity to highlight only the spectral distribution in this energy region. Here we see that the in-core facility actually has a harder spectrum, due primarily to the high-energy fission neutrons within the core. For the FNI sample volume, the very high-energy neutrons have been essentially eliminated during transit through the shield and filter regions of the FNI facility. There is still a large fast flux, but the peak of the neutron spectrum is in the 0.2 MeV region rather than in the 1 MeV range as seen for the core irradiation positions. This downward shift in the high-energy spectrum is why the RDF is lower in the FNI relative to the in-core D2 location. Since the

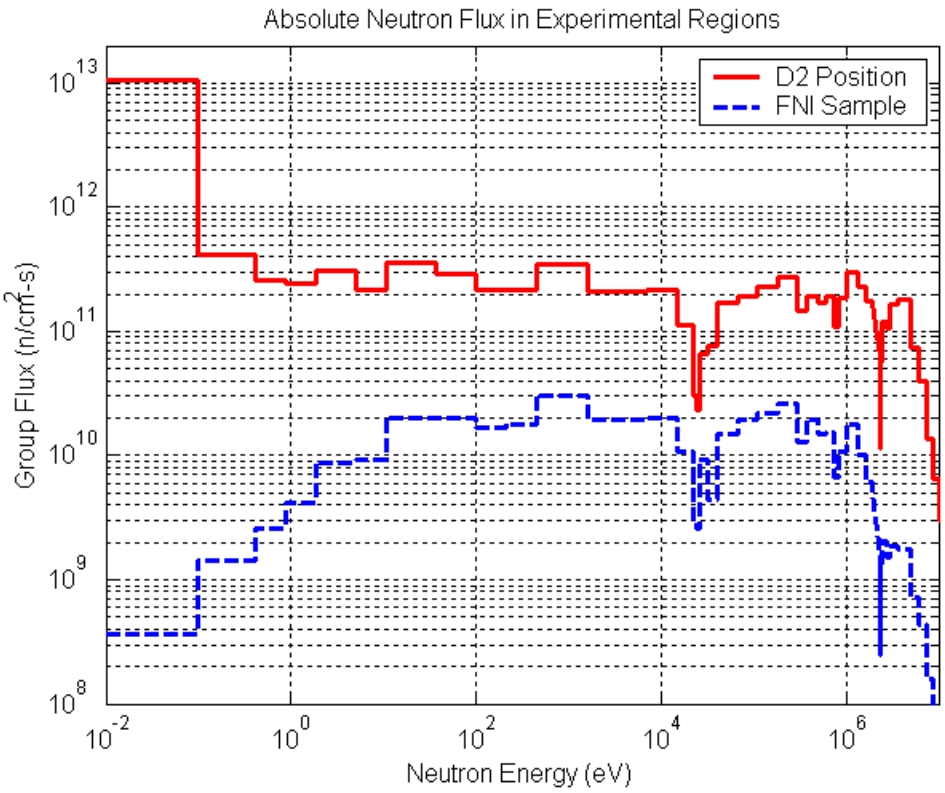

Fig. 15a Absolute neutron flux in two experimental facilities within the UMLRR.

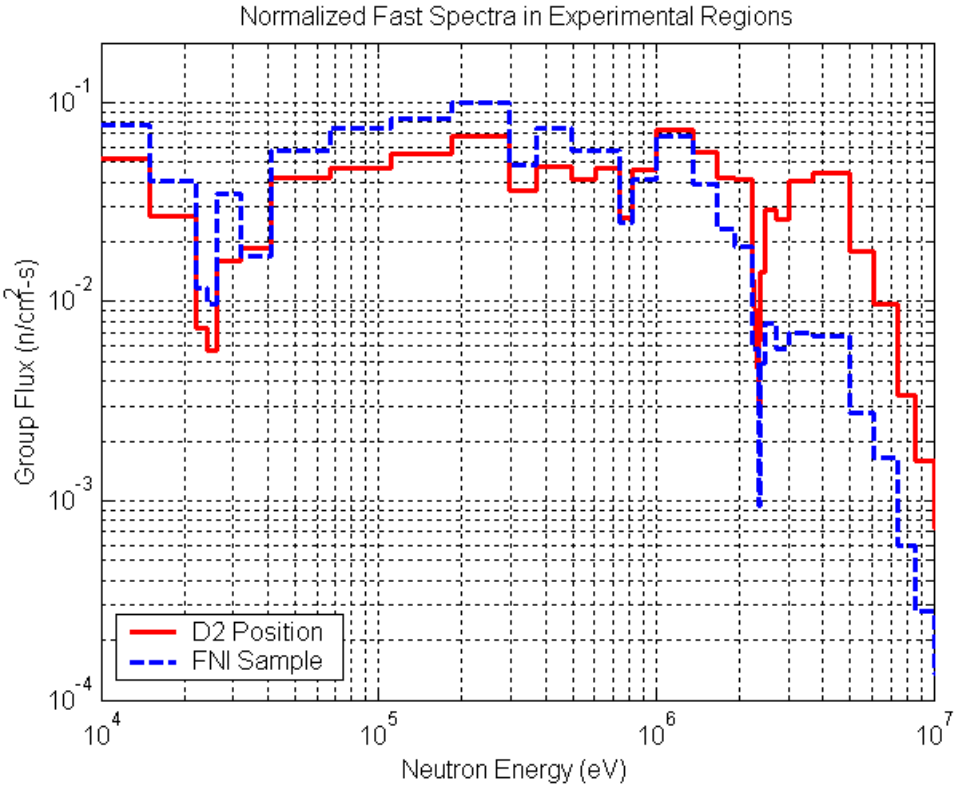

Fig. 15b Normalized fast neutron spectra within the D2 and FNI regions.

silicon kerma factors tend to decrease at lower energies, this indicates that a higher fluence of neutrons with spectral profile $\phi(E)$ is needed to cause the same number of atomic displacements that a unit fluence of 1 MeV neutrons would cause.

For example, in the FNI, the fast flux > 0.01 MeV is about 2.5×10^{11} n/cm^2-s. But, because of the softer spectrum, this would give the same number of displacements in silicon as about 1.4×10^{11} n/cm^2-s of 1 MeV neutrons. Thus, the 1 MeV equivalent flux indicator tries to factor out differences in neutron spectrum by comparing the affect of the full fast spectrum, rather than just the magnitude of the fast flux. The 1 MeV equivalent flux, therefore, is a better measure of performance, since it quantifies both the magnitude and composite affect of the fast neutron distribution on the irradiated material.

The average parameters in Table 2 give a good snapshot of the radiation environments within the in-core D2 position and the ex-core FNI sample volume. However, since the FNI sample region is so large, it is also important to characterize the spatial distribution of the key indicators within this region. Recall that a real effort was made in the design of the composite FNI facility to assure a relatively uniform distribution throughout the sample. If this goal is reached, then the average values in Table 2 will be applicable (approximately) over the whole sample.

The best way to visualize the full spatial distribution within the sample region is through a series of 2-D color contour maps that show the flux or fluence magnitude at each x,y or y,z point in the region of interest. Here we have chosen to present the 1 MeV equivalent fluence distributions obtained from the XY and YZ DORT models. In both cases, the average fluence was set at 10^{15} n/cm^2 which, based on the observed average 1 MeV equivalent flux, equates to a two hour irradiation interval. Also, since we envision that a single 180^o rotation will be needed to minimize the fast flux attenuation through the thickness of the sample, both cases, with and without the sample rotation, are included.

The 2-D spatial distributions are presented in Figs. 16 and 17, respectively, for the XY and YZ models. The upper portion of each figure contains the fluence profile assuming no rotation, and the lower figure includes the composite distribution with a 180^o rotation at the midpoint of the irradiation interval. Since the current analysis is focused on a empty sample canister -- to characterize the unperturbed flux profiles in the experimental volume -- one would not expect significant attenuation through the sample (y-direction in the DORT models). However, even in the sample-free case, the top portions of Figs. 16 and 17 show noticeable decreases in the 1 MeV equivalent fluence through the sample. In these cases the maximum–to-minimum fluence within the sample region (highlighted area in the plots) is as high as 1.3-1.4, which clearly exceeds the $\pm$ 10% uniformity criterion from the original design goals. However, as apparent from the lower plots in Figs. 16 and 17, if the sample canister is rotated at the midpoint of the irradiation period, a very uniform fluence distribution can be obtained. For the 1 MeV equivalent fluence, the maximum-to-minimum ratio drops below 1.10 in both the XY and YZ models for the sample-free canister. This clearly supports the argument for a 180^o rotation at the midpoint of the irradiation cycle.

As a more quantitative measure of the 1 MeV equivalent fluence distribution, simple plots of the fluence profiles along the centerlines of the sample region are also given in Figs. 18 and 19. These data include the single sample rotation at the middle of the irradiation interval. Figure 18 shows the y-profile from front to back and the x-profile from left to right as obtained from the DORT XY model. Similarly, Fig. 19 shows the z-directed bottom to top distribution and the y-directed distribution from back to front from the YZ model. Note that the y-profiles from the two models agree quite closely. These figures quantify the x,y,z fast fluence distribution within the sample, and they clearly show that the uniformity criteria are satisfied in all three directions.

As a final summary characterization of the sample region, the average values and the maximum-to-minimum, maximum-to-average, and minimum-to-average ratios for the fast and thermal fluence profiles and the gamma dose distribution for the final FNI design are included in Table 3. These data also quantify the magnitude and uniformity of the various distributions in both the XY and YZ DORT models. As apparent, all the profiles are quite uniform, but the thermal fluence and the gamma dose do show slightly more variability than the fast fluence profiles. However, even with the slightly higher maximum-to-average ratios, the peak values of the thermal fluence and gamma dose are well below the pre-set design criteria. Thus, it appears that the current FNI design meets or exceeds all the specifications set at the early stages of this project.

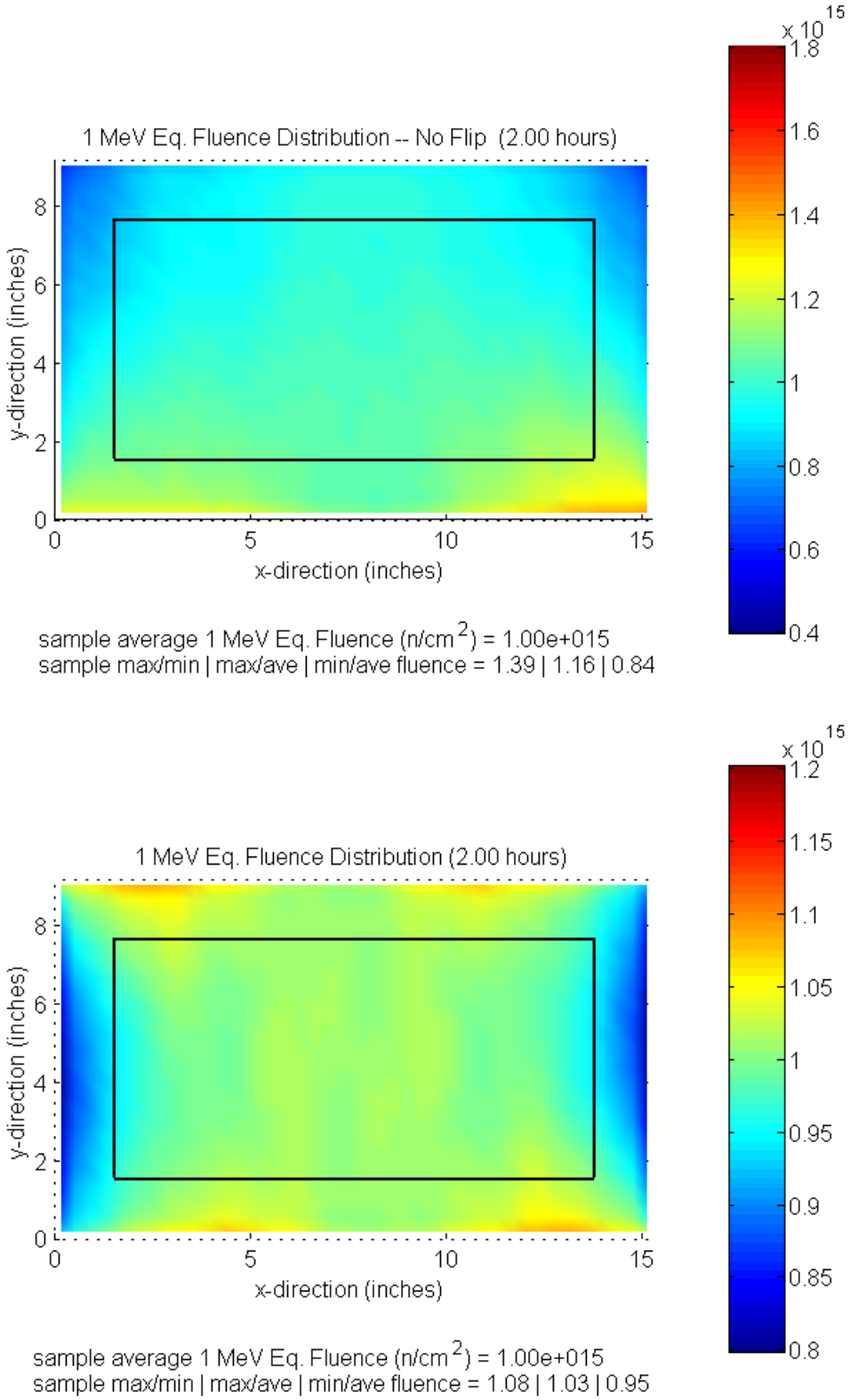

Fig. 16 XY spatial 1 MeV equivalent fluence distribution in the FNI canister.

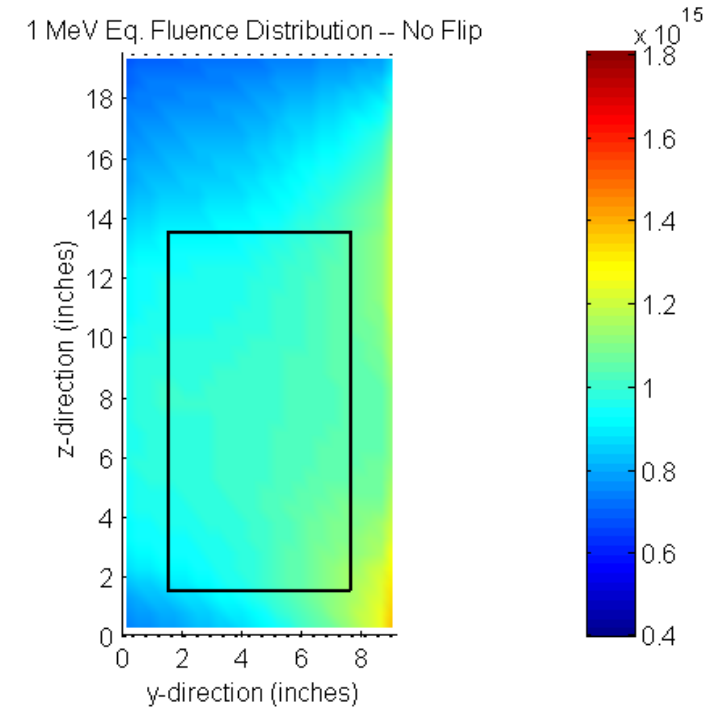

sample average 1 MeV Eq. Fluence (n/cm^2) = 1.00e+015
sample max/min | max/ave | min/ave fluence = 1.28 | 1.13 | 0.88

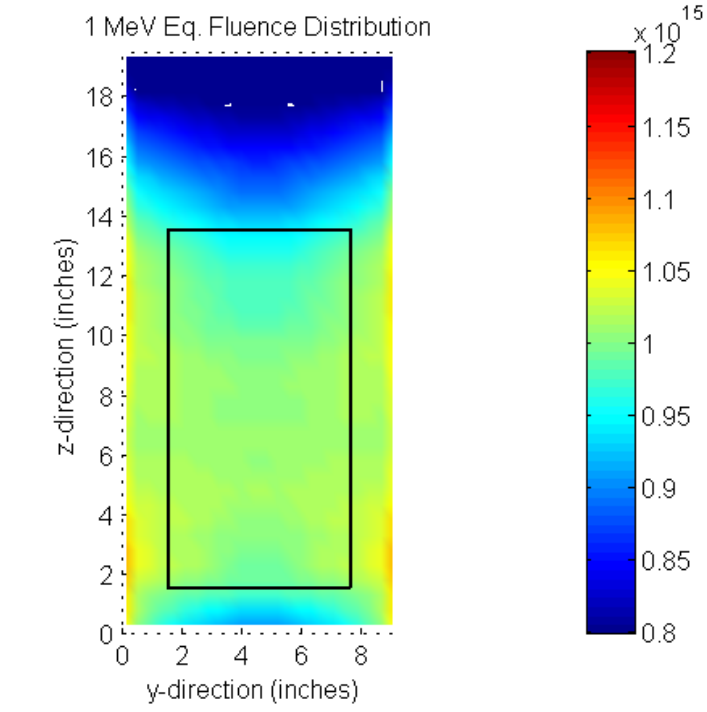

sample average 1 MeV Eq. Fluence (n/cm^2) = 1.00e+015
sample max/min | max/ave | min/ave fluence = 1.08 | 1.02 | 0.95

Fig. 17 YZ spatial 1 MeV equivalent fluence distribution in the FNI canister.

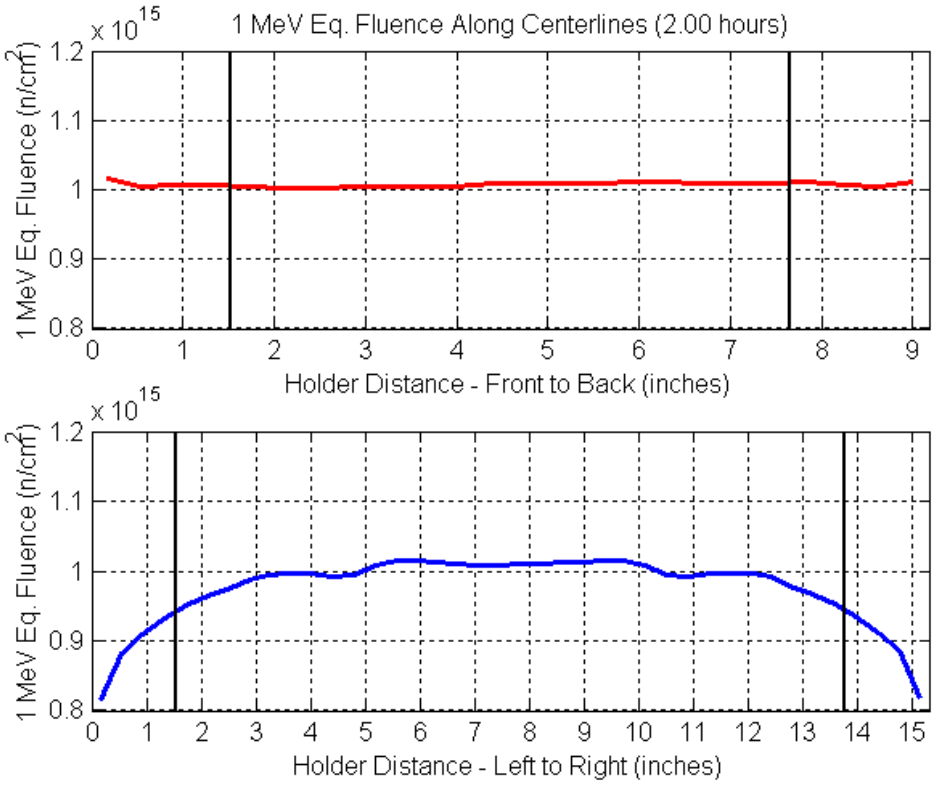

Fig. 18 1 MeV equivalent fluence profiles along centerlines of the FNI in the XY model.

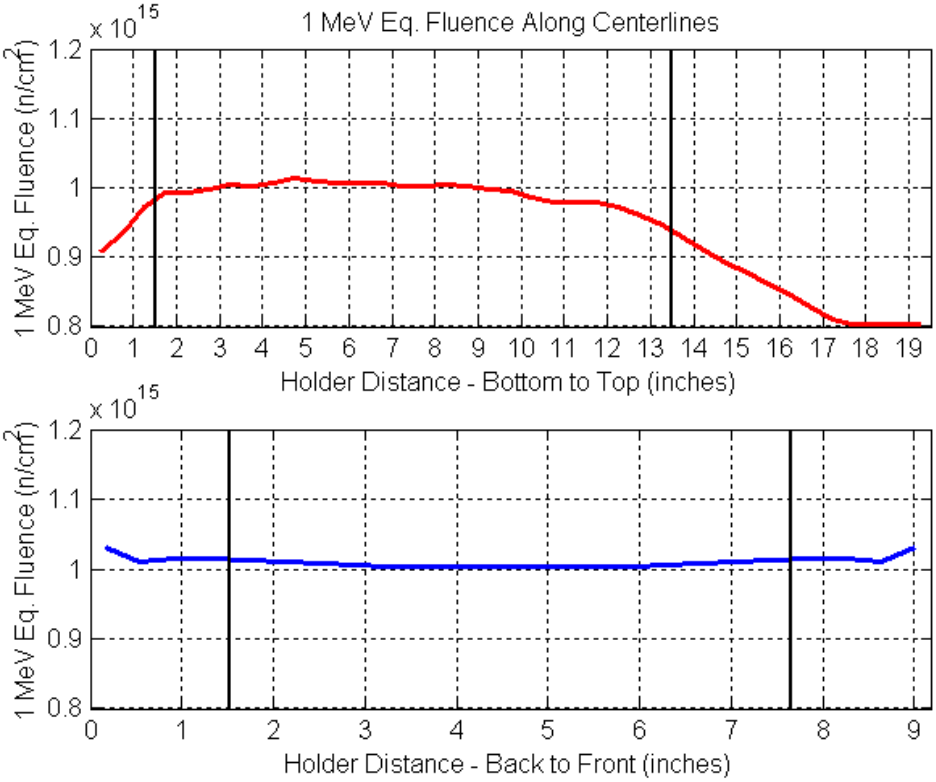

Fig. 19 1 MeV equivalent fluence profiles along centerlines of the FNI in the YZ model.

Table 3. Summary uniformity information for several distributions in the XY and YZ models (2 hour irradiation time with midpoint rotation)

Parameter	XY Model	YZ Model
1 MeV Equivalent Fluence (n/cm^2)		
sample average	1.00E+15	1.00E+15
max/min	1.08	1.08
max/ave	1.03	1.02
min/ave	0.95	0.95
Thermal Neutron Fluence (n/cm^2)		
sample average	3.48E+13	3.69E+13
max/min	1.12	1.15
max/ave	1.04	1.04
min/ave	0.92	0.91
Gamma Dose to Silicon (Krad)		
sample average	92.2	131
max/min	1.21	1.16
max/ave	1.09	1.08
min/ave	0.90	0.93

V. PRELIMINARY TESTING

The above section gives detailed computational results for the new ex-core fast neutron irradiator. Unfortunately, however, we do not yet have much experimental data to validate all these design calculations. An experimental characterization effort for the FNI facility has just recently been initiated (Feb. 2002), but no useful information is available as yet. However, during startup of the new core configuration, a series of blade worth measurements were made. In addition, a single foil irradiation test was recently performed in the radiation basket in the in-core D2 location. Although very limited in scope, these two tests can provide some initial experimental evidence to support the design methodology used in this work.

A preliminary analysis of the data from the blade worth measurements and the foil irradiations in position D2 has been made, and these initial results have been compared to VENTURE and DORT computations of these quantities. Some summary results from these initial comparisons are given in Tables 4 and 5.

In particular, the VENTURE-calculated blade worths are tabulated along with the measured values in Table 4. As apparent, both the magnitude and worth distribution for Blades 1-4 agree reasonably well. This is consistent with previous experience, since we have traditionally done reasonably well at predicting the blade worths with our 2-D VENTURE models. This new test does show, however, that the predicted tilting of the blade worth distribution (and flux distribution) towards Blade 4 is real, and it suggests that the in-core power and fission source distributions computed within our VENTURE 2-D XY model is probably representative of the actual system. These results also validate, to some extent, some of the safety analyses performed for the post FNI facility.

Table 4. Comparison of measured and calculated blade worths for the M-2-5 core

Parameter	Measured %Δk/k	Calculated %Δk/k
Blade 1 Worth	2.82	2.87
Blade 2 Worth	2.19	2.14
Blade 3 Worth*	3.19	2.99
Blade 4 Worth	3.93	3.96

* The experimental uncertainty was unusually large for this measurement.

In our first routine test within the new post-FNI configuration (the M-2-5 core and FNI layout), a set of activation foils were placed in the central region of a standard experimental bayonet and inserted within the radiation basket in position D2 for a period of 7.5 minutes. The reactor was operating at a steady-state power level of 1 kW. After removal and counting, the measured count rates were converted to saturated activities normalized to a nominal 1 MW power level. These data were then compared to the normalized reaction rates (reactions/sec per atom) computed using the zone-averaged fluxes from the DORT XY model. The 47-group reaction cross sections for these calculations were taken directly from the BUGLE-96 response library.[9]

The results from this initial comparison are summarized in Table 5. Note that the Zn64 n,p reaction rate was not computed because the appropriate reaction cross sections were not readily available. Appropriate data for the three remaining reactions were available, however, and the calculated-to-experimental ratios for these

Table 5. Comparison of measured and calculated foil activities in the D2 position

Reaction	Threshold Energy (MeV)	Experimental Activity (dps/atom)	Calculated Activity (dps/atom)	C/E Ratio
In115 (n,n') In115m	1.2	4.22E-13	4.38E-13	1.04
Ti47 (n,p) Sc47	2.2	4.65E-14	5.32E-14	1.14
Zn64 (n,p) Cu64	2.8	1.11E-13	---	---
S32 (n,p) P32	2.9	1.76E-13	1.53E-13	0.87

cases are all within ±15% of unity. This level of uncertainty is consistent with the experimental uncertainty and our ability to routinely compute the fast neutron spectrum in similar situations (typical C/E values within 10-20% of unity are considered acceptable and consistent with standard practice). Thus, these initial results are promising, and they indicate some level of self-consistency within the basic modeling methodology. However, the available experimental data for verification are very limited, and there are no direct measurements as yet for the FNI facility. Thus, it is simply too early to pass judgment concerning the adequacy of the methodology and the overall design of the new ex-core irradiator.

VI. CONCLUSIONS/FUTURE WORK

The goal of this work was to design, build, and test a new large-volume fast neutron irradiator for use within the UMass-Lowell research reactor (UMLRR). The new irradiator accommodates a nominal 12"x12"x6" sample size with a 1 MeV equivalent flux greater than 10^{11} n/cm^2-s and relatively low thermal neutron and gamma background levels.

The first two phases of the work are complete and this paper presents a detailed summary of many of the physical design characteristics and much of the VENTURE and DORT computational analyses used to support the fast neutron irradiator (FNI) that was actually constructed and installed within the pool of the UMLRR. The third task, the testing and verification of the as-built facility, has only recently been initiated. This task will be completed over the next few months. Routine operation of the new facility should begin in April or May 2002.

REFERENCES

1. "FSAR Supplement for Conversion to Low Enrichment Uranium (LEU) Fuel," submitted to the NRC for conversion of the UMass-Lowell Research Reactor (May 1993).

2. J. R. White, et. al., "Calculational Support for the Startup of the LEU-Fueled UMass-Lowell Research Reactor," Advances in Reactor Physics and Mathematics and Computation, Pittsburgh, PA (May 2000).

3. J. R. White, et. al., "Preliminary Characterization of the Irradiation Facilities within the LEU-Fueled UMass-Lowell Research Reactor," Advances in Reactor Physics and Mathematics and Computation, Pittsburgh, PA (May 2000).

4. "VENTURE-PC - A Reactor Analysis Code System," Radiation Safety Information Computational Center, CCC-654 (1997).

5. "DOORS3.1 - One, Two, and Three Dimensional Discrete Ordinates Neutron/Photon Transport Code System," Radiation Safety Information Computational Center, CCC-650 (1996).

6. "Proposed Technical Specifications for the University of Massachusetts Lowell Reactor with Low Enrichment Fuel," submitted to the NRC for conversion of the UMass-Lowell Research Reactor (May 1993).

7. "SCALE 4.3 - Modular Code System for Performing Standardized Computer Analyses for Licensing Evaluation for Workstations and Personal Computers," Radiation Safety Information Computational Center, CCC-545 (1997).

8. "VITAMIN-B6 - A Fine-Group Cross Section Library Based on ENDF/B-VI Release 3 for Radiation Transport Applications," Radiation Safety Information Computational Center, DLC-184 (1996).

9. “BUGLE-96 - Coupled 47 Neutron, 20 Gamma-Ray Group Cross Section Library from ENDF/B-VI for LWR Shielding and Pressure Vessel Dosimetry Applications,” Radiation Safety Information Computational Center, DLC-185 (1996).

10. “Characterizing Neutron Energy Fluence Spectra in Terms of an Equivalent Monoenergetic Neutron Fluence for Radiation-Hardness Testing of Electronics,” ASTM Standard Practice E722-85 (1985).